REPORT DOCUMENTATION PAGE

Form Approved
OMB NO. 0704-0188

1. AGENCY USE ONLY (Leave Blank)	2. REPORT DATE 12/r13/01	3. REPORT TYPE AND DATES COVERED Final, 15 March 1998 - ~~20 September~~ 2001 30Jun01

4. TITLE AND SUBTITLE
Terahertz Plama Wave Electronics

5. FUNDING NUMBERS
DAAG55-98-1-0131

6. AUTHOR(S)
Michael Shur

7. PERFORMING ORGANIZATION NAME(S) AND ADDRESS(ES)
Rensselaer Polytechnic Institute
110 8th St., Troy, NY 12180

8. PERFORMING ORGANIZATION REPORT NUMBER

9. SPONSORING / MONITORING AGENCY NAME(S) AND ADDRESS(ES)
U. S. Army Research Office
P.O. Box 12211
Research Triangle Park, NC 27709-2211

10. SPONSORING / MONITORING AGENCY REPORT NUMBER
37725.6-EL

11. SUPPLEMENTARY NOTES
The views, opinions and/or findings contained in this report are those of the author(s) and should not be construed as an official Department of the Army position, policy or decision, unless so designated by other documentation.

12 a. DISTRIBUTION / AVAILABILITY STATEMENT
Approved for public release; distribution unlimited.

12 b. DISTRIBUTION CODE

13. ABSTRACT (Maximum 200 words)

We performedt an experimental and theoretical study of nonresonant detection of sub-terahertz radiation in GaAs/AlGaAs and GaN/AlGaN heterostructure field effect transistors. The experiments were performed in a wide range of temperatures (8-300K) and for frequencies ranging from 100GHz to 600GHz. The photoresponse measured as a function of the gate voltage exhibited a maximum near the threshold voltage. The results were interpreted using a new theoretical model that shows that the maximum in photoresponse can be explained by the combined effect of exponential decrease of the electron density and the gate leakage current.

14. SUBJECT TERMS
Terahertz Detector, Terahertz Plasma Wave Electronics, GaAs HFET

15. NUMBER OF PAGES
~~0~~ 14

16. PRICE CODE

17. SECURITY CLASSIFICATION OR REPORT	18. SECURITY CLASSIFICATION ON THIS PAGE	19. SECURITY CLASSIFICATION OF ABSTRACT	20. LIMITATION OF ABSTRACT
UNCLASSIFIED	UNCLASSIFIED	UNCLASSIFIED	UL

REPORT DOCUMENTATION PAGE (SF298)
(Continuation Sheet)

See next attached pages for a full report:

Final Report for Grant DAAG55-98-1-0131
(Continuation Sheet for SF298)

Introduction

In a normal regime, the upper operation frequency of a Field Effect Transistor (FET) - fT, is limited by the electron transit time t_0 ($f_T \cong 1/2\pi\, t_0$ -see for example[1]). However, plasma effects become important in modern, short channel field effect transistors, where the sheet carrier density is very high. These effects are expected to allow the use of FETs at much higher frequencies – reaching even the terahertz range for submicron devices[2].

Plasma waves with a linear dispersion law, $\omega(k) = sk$, may propagate in a FET channel. Here s is the plasma wave velocity that depends on carrier density, and k is the wave vector. The velocity of the plasma waves, s, is typically on the order of 10^8 cm/s, which is much larger than the drift velocity of the two-dimensional (2D) electrons in the FET channel. This is why the propagation of plasma waves can be used for new regimes of FET operation, with a much higher frequency than for conventional, transit-time limited devices.

In a FET with a given length L the values of plasma frequencies are discrete and given by[2] $\square_N = \omega_0\,(1+2N)$, where $\omega_0 = \pi s/2L$, and N= 0, 1, 2,.... Allen et al. [3] observed infrared absorption, and Tsui et al. [4] reported on weak infrared emission related to such plasma waves in silicon inversion layers. Burke et al. showed that the impedance of a high mobility transistor exhibits maxima at the fundamental plasma frequency and its harmonics. [5]

Under certain conditions, plasma oscillations can be excited in a FET by a dc current[2], and the FET can be used as an oscillator operating in the terahertz range[6]. Nonlinear properties of the plasma waves can be utilized for terahertz detectors, broadband detectors, mixers, and frequency multipliers [7,8].

A FET, biased by the gate-to-source voltage and subjected to electromagnetic radiation, can develop a constant drain-to-source voltage, which has a resonant dependence on the radiation frequency $f=\omega/2\pi$ with the maxima at the plasma oscillation frequencies $f_N=\omega_N/2\pi$ [7,8]. The plasma wave velocity depends on the carrier density in the channel , n ,and the gate to channel capacitance per unit area C, $s=(e^2n/mC)^{1/2}$, where e is the electron charge, m is the electron effective mass. In the gradual channel approximation, the carrier density in the channel is related to the gate voltage as $n=CU_0/e$. U_0 is the gate to channel voltage swing that is defined as $U_0=U_g - U_{th.}$, where U_g is the gate voltage and U_{th} is the threshold voltage. In this case, the fundamental plasma frequency can be expressed by an approximate relation $f_o=\omega_0/2\pi=(eU_0/m)^{1/2}/4L$. This relation leads to two important consequences: i) a sufficiently short (sub-micron) FET can operate as a THz detector and ii) the frequency of this detector can be tuned by the gate voltage. The width of the resonance curve is determined by the inverse time of the electron momentum relaxation, $1/\tau$. The dimensionless parameter, which governs the physics of the problem *is* $\omega_0\tau$. In the regime such that $\omega_0\tau>>1$, the FET operates as a resonant detector. When $\omega_0\tau<<1$, the plasma oscillations are overdamped, and the FET response is a smooth function of ω as well as of the gate voltage (non-resonant broadband detection).

The non-resonant detection at both terahertz and sub-terahertz frequencies has been reported in several papers [9] but its behavior could not be fully understood especially in the range of the gate voltages close to the threshold voltage.

In Fig.1, we show a few examples of typical experimental data. The drain–source voltage photoinduced by the 600 GHz radiation in GaAs/AlGaAs FET, is shown as a function of the gate voltage, U_g. The experimental results can be well explained by the previous theory[8] only for relatively large positive gate voltage swings, U_0, for which the detector response decays as $1/U_0$. However, at the gate voltages close to the threshold (small values of U_0), the experimental data deviate from the theoretical curves. Moreover, for U_g smaller than the threshold voltage (negative values of U_0), the experimentally observed response decreases, so that the response always reaches a maximum value close to the FET threshold. This feature cannot be explained by the previous detector model [8].

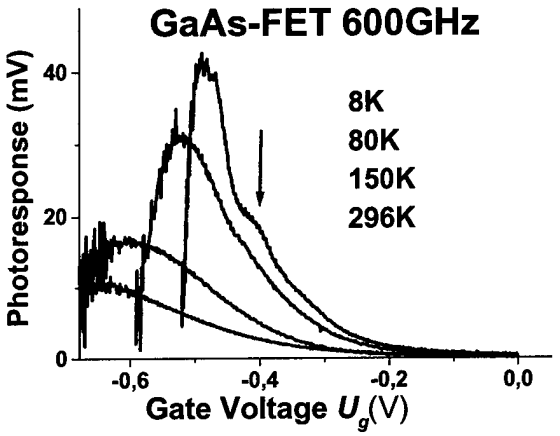

Fig.1 Measured photoresponse of the GaAs/AlGaAs 0.15μm FET for the 600GHz radiation. Radiation induced source - drain voltage as a function of the gate voltage U_g is shown for temperatures 8K, 80K, 150K, 296K. The arrow marks the maximum corresponding to the resonant detection observed at the lowest temperature 8K.

In this paper, we focus on the experimental and theoretical study of the nonresonant detection under the conditions $\omega_0\tau<1$ and $\omega\tau<1$. We present experiments performed on FETs made of two different semiconductor systems, GaAs/AlGaAs and GaN/AlGaN, in a wide range of temperatures (8-300K) and for frequencies ranging from 100GHz to 600GHz. The results are interpreted using a new theoretical model, which describes the photoresponse below and above the transistor threshold. The model shows that the gate leakage current suppresses the detector response in the sub-threshold region leading to a nonresonant maximum in photoresponse versus gate dependence.

At the lowest temperature (8K), one can also see a resonant feature in the response (marked by an arrow) that is superimposed on the broad background. It is due to a resonant detection of 600GHz radiation. The resonant response appears at lowest temperatures, since, at these temperatures, the electron scattering time increases and we reach $\omega_0\tau=1$ - the resonant detection condition. The resonant detection was described in more details in Ref.[9].

Theory of subthreshold nonresonant detection

The theory presented in Ref.7 was developed assuming that $eU_0>>k_BT$, where k_B is the Boltzmann constant and T is temperature. For U_0 approaching zero (i.e. the gate voltage approaching the threshold voltage), the model predicted that the photoresponse signal should diverge as $(1/U_0)$. In this work, we will make an attempt to generalize the theory[7] for the case of an arbitrary gate voltage. Here we restrict ourselves to nonresonant case assuming that $\omega_0\tau<1$ and $\omega\tau<1$. The key point is taking into account the leakage current from the metal gate to the 2D electron gas in the channel.

Well above threshold, the gate leakage is small compared to the current in the channel and does not affect the response of the detector[10] .

However, for negative values of U_0, when electron concentration in the FET channel becomes exponentially small, the leakage current plays an important role and should be taken into account.

The general equation for the electron concentration in the FET channel is given by [1]

$$n = n^* \ln\left[1 + \exp\left(\frac{eU_0}{\eta k_B T}\right)\right]. \qquad (1)$$

Here $n^* = \frac{C\eta k_B T}{e^2}$, C is the gate capacitance per unit area and η is the ideality factor. For large positive values of gate voltage ($U_0 > \frac{\eta k_B T}{e}$) the electron concentration in the FET channel increases with the gate voltage swing as $n = \frac{CU_0}{e}$.

In the opposite case of large negative gate voltage swings, $U_0 < 0$, $|U_0| > \frac{\eta k_B T}{e}$, the electron concentration is exponentially small

$$n = n^* \exp\left(\frac{eU_0}{\eta k_B T}\right). \qquad (2)$$

First, we will find the analytical expression for detector response valid for the case $U_0<0$. Then we generalize this expression for the case of arbitrary values of U_0.

We start with the hydrodynamic equations, which describe the 2D electrons in the FET channel [2]

$$\frac{\partial v}{\partial t} + v\frac{\partial v}{\partial x} + \frac{v}{\tau} + \frac{e}{m}\frac{\partial u}{\partial x} = 0, \qquad (3)$$

$$\frac{\partial n}{\partial t} + \frac{\partial (nv)}{\partial x} = 0. \qquad (4)$$

Here u is the local value of voltage, $\frac{\partial u}{\partial x}$ is the longitudinal electric field in the FET channel, v is the electron velocity. We assume that the relation between local concentration n and local voltage u is given by Eq.(1) with replace U_0 by u. In Eq.(3) we will neglect $\frac{\partial v}{\partial t} + v\frac{\partial v}{\partial x}$. The term $\left(\frac{\partial v}{\partial t}\right)$ is small compared with $\left(\frac{v}{\tau}\right)$ since $\omega\tau << 1$. The criterion of neglecting $v\frac{\partial v}{\partial x}$ will be evaluated later. We will also need to add the gate leakage current, j_0, into the right hand side of Eq. (4). As a result, we get the following system of two equations

$$v = -\frac{e\tau}{m}\frac{\partial u}{\partial x}, \qquad (5)$$

$$\frac{\partial n}{\partial t} + \frac{\partial (nv)}{\partial x} = j_0 / e, \qquad (6)$$

where Eq.(5) is Ohm's law, and Eq.(6) is the continuity equation. In what follows we assume j_0 = const. Eqs.(5, 6) should be solved together with Eq. (2) using the following boundary conditions (which are the same as used in Refs.[2,6,7])

$$u\big|_{x=0} = U_0 + u_a \cos(\omega t) \qquad (7a),$$

$$v\big|_{x=L} = 0 \qquad (7b).$$

Here U_0 is the dc gate-to-source voltage swing, $u_{ac}=u_a \cos(\omega t)$ is the external ac voltage induced between the gate and source by the incoming electromagnetic radiation.
The condition (7b) corresponds to zero drain current.

Next, we will show that electromagnetic radiation induces the dc drain-to-source voltage, $\Delta u = \left\langle u\big|_{x=L} - u\big|_{x=0} \right\rangle$,which is called detector response (the angular brackets denote averaging over time). From Eqs. (2),(5) we get

$$v = -\frac{s_0^2 \tau}{n}\frac{\partial n}{\partial x}, \qquad (8)$$

where

$$s_0 = \sqrt{\frac{\eta k_B T}{m}} \qquad (9)$$

Substituting (8) into (6) we obtain:

$$\frac{\partial n}{\partial t} - s_0^2 \tau \frac{\partial^2 n}{\partial x^2} = j_0 / e \qquad (10)$$

The boundary conditions for Eq. (10) are obtained from Eqs. (2), (5), and (7)

$$n\big|_{x=0} = n^* \exp\left(\frac{e(U_0 + u_a \cos\omega t)}{\eta k_B T}\right), \qquad (11)$$

$$\left.\frac{\partial n}{\partial x}\right|_{x=L} = 0. \qquad (12)$$

Following the method of Ref. [8] we will search for a solution in the form of a series with respect to the small amplitude of the ac wave u_a. The leading term in the expansion of the detector response is proportional to the intensity of the electromagnetic wave, $\Delta u \sim (u_a)^2$. This allows us to neglect the terms containing u_a in the powers higher than two. Expanding Eq. (11) with respect to u_a up to the second order yields

$$n\big|_{x=0} = n^* \left[1 + \frac{eu_a}{T}\cos\omega t + \left(\frac{eu_a}{\eta k_B T}\right)^2 \frac{1}{2}\cos^2 \omega t\right] \exp\left(\frac{eU_0}{\eta k_B T}\right). \qquad (13)$$

One can show that the second harmonic with the frequency 2ω leads to the contribution to the response on the order of $(u_a)^4$. Neglecting the second harmonic, we get from Eq. (13):

$$n\big|_{x=0} \approx n^* \left[1 + \left(\frac{eu_a}{2\eta k_B T}\right)^2 + \frac{eu_a}{\eta k_B T}\cos\omega t\right] \exp\left(\frac{eU_0}{\eta k_B T}\right). \qquad (14)$$

The solution of Eq. (10) with boundary conditions (12), (14) is given by

$$n = n^*\left(1+\left(\frac{eu_a}{2\eta k_B T}\right)^2\right)\exp\left(\frac{eU_0}{\eta k_B T}\right) + \frac{j_0}{{s_0}^2\tau e}\left(xL-\frac{x^2}{2}\right)+\frac{eu_a n^*}{2\eta k_B T}\exp\left(\frac{eU_0}{\eta k_B T}\right)\left\{\frac{ch(q[L-x])}{ch(qL)}e^{i\omega t}+\frac{ch(q^*[L-x])}{ch(q^*L)}e^{-i\omega t}\right\} \quad (15)$$

Where $q=\sqrt{\frac{i\omega}{{s_0}^2\tau}}$, $q^*=\sqrt{\frac{-i\omega}{{s_0}^2\tau}}$ (16)

The drain voltage $u\big|_{x=L}$ is determined using Eq. (2)

$$u\big|_{x=L}=\frac{\eta k_B T}{e}\ln\frac{n\big|_{x=L}}{n^*} \quad (17)$$

Substituting (15) into (17) yields

$$u\big|_{x=L}=U_0+\frac{\eta k_B T}{e}\ln\left\{1+\left(\frac{eu_a}{2\eta k_B T}\right)^2+\frac{j_0 L^2}{2{s_0}^2\tau e n^*}+\frac{eu_a}{2\eta k_B T}\left\{\frac{e^{i\omega t}}{ch(qL)}+\frac{e^{-i\omega t}}{ch(q^*L)}\right\}\right\} \quad (18)$$

Expanding the logarithm with respect to u_a, averaging over t, and keeping only the terms which depend on u_a, we obtain the following expression for the detector response

$$\left\langle u\big|_{x=L}-u\big|_{x=L}\right\rangle=\frac{{eu_a}^2}{4m{s_0}^2}\left\{\frac{1}{1+\kappa\exp\left(-\frac{eU_0}{\eta k_B T}\right)}-\frac{1}{\left(1+\kappa\exp\left(-\frac{eU_0}{\eta k_B T}\right)\right)^2 ch(qL)ch(q^*L)}\right\}, \quad (19)$$

where

$$\kappa=\frac{j_0 L^2 me}{2C\tau\eta^2 k_B^2 T^2} \quad (20)$$

is a dimensionless parameter, which is assumed to be small ($\kappa \ll 1$).
Eq (19) is valid for $U_0<0$. An analogous equation, which is valid for an arbitrary sign of U_0, is obtained from (19) by replacing s_0 with the plasma wave velocity s, which is given by

$$s^2=\frac{e}{m}\frac{n}{(dn/du)}\bigg|_{u=U_0}.$$

Using Eq.(1) we get

$$s^2={s_0}^2\left(1+\exp\left(-\frac{eU_0}{\eta k_B T}\right)\right)\ln\left(1+\exp\left(\frac{eU_0}{\eta k_B T}\right)\right). \quad (21)$$

In the limiting cases, Eq. (21) yields

$s^2=\frac{eU_0}{m}$, for $eU_0>\eta k_B T$;

$s^2 = s_0^2$, for $U_0<0$ and $e|U_0| > \eta k_B T$.

Finally, we get the following expression for the detector response

$\Delta u =$

$$= \frac{eu_a^2}{4ms^2}\left\{\frac{1}{1+\kappa\exp\left(-\frac{eU_0}{\eta k_B T}\right)} - \frac{1}{\left(1+\kappa\exp\left(-\frac{eU_0}{\eta k_B T}\right)\right)^2\left[sh^2 Q+\cos^2 Q\right]}\right\}, \quad (22)$$

where $Q = \sqrt{\frac{\omega}{2\tau}}\frac{L}{s}$. Eq (22) is valid for an arbitrary sign of U_0. For $U_0>0$ it reduces to Eqs. (23) and (33) in Ref.[7,8].

The dependence of the photoresponse on the basic parameters can be more easily seen in the case of "long samples", such that (Q>>1). In this case, Eq.22 simplifies to

$$\Delta u = \frac{eu_a^2}{(4\eta k_B T)}\frac{1}{\left(1+\exp\left(-\frac{eU_0}{\eta k_B T}\right)\right)\left(1+\kappa\exp\left(-\frac{eU_0}{\eta k_B T}\right)\right)\ln\left(1+\exp\left(\frac{eU_0}{\eta k_B T}\right)\right)}. \quad (23)$$

For $eU_0>>\eta k_B T$, we have

$$\Delta u = \frac{u_a^2}{4U_0}. \quad (24)$$

For $U_0<0$ $\kappa\exp\left(-\frac{eU_0}{\eta k_B T}\right) >> 1$, Eq. (23) yields

$$\Delta u = \frac{eu_a^2}{4\eta k_B T\kappa}\exp\left(-\frac{e|U_0|}{\eta k_B T}\right). \quad (25)$$

We see that response has a maximum for $eU_0 \approx -\frac{\eta k_B T}{2}\ln\left(\frac{1}{\kappa}\right)$. The maximum value of response is given by

$$\Delta u_{\max} \approx \frac{eu_a^2}{4\eta k_B T} \quad (26)$$

It can also be shown that the width of the peak is proportional to $\eta k_B T \ln(1/\kappa)$.

So, one can see that the crucial parameter that defines the position and the value of the maximum is $\eta k_B T$. The value of the maximum photoresponse does not depend on the leakage current but only on the factor $\eta k_B T$. The position and the width of the maximum depend on both ($\eta\, k_B T$ and κ) parameters but the value of $\eta k_B T$ is the most important factor as ($\ln\frac{1}{\kappa}$) is a slowly varying function of j_0.

In deriving Eqs. (22-26) from Eqs. (3,4) we neglected the term *vdv/dx*. One can show that neglecting this term is valid when $\kappa \exp\left(-\frac{eU_0}{\eta k_B T}\right) < \frac{L}{s_0 \tau}$. Estimates show that in our experiments $L/s_0\tau >> 1$. Hence, the response in the range of negative U_0 decreases according to Eq (23) up to the values $\Delta u \approx \Delta u_{\max} \frac{s_0\tau}{L} << \Delta u_{\max}$. For smaller values of the response, Eqs. (22-26) are no longer valid.

Fig. 2 shows the response predicted by Eq. (22) for different values of the leakage current and temperatures. The parameters were chosen to correspond to typical values for 0.15μm-gate GaAs based FETs.

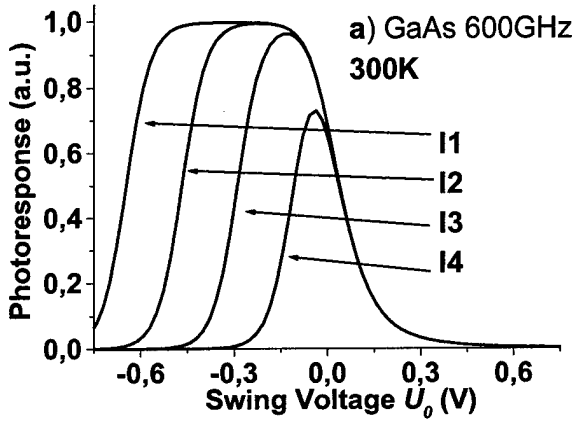

(a)

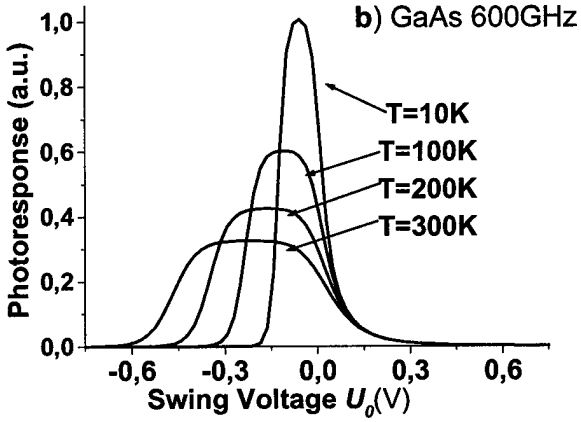

(b)

Fig.2. Photoresponse of the GaAs/AlGaAs FET at 600GHz - as calculated according Eq.22. a) response at T=300K and for η=1.5, for four different leakage currents. I1 corresponds to the current density j_0=1.3*10A/m^2, I2 - j_0=1.3*10^{3}A/m^2, I3- j_0= 1.3*10^{5}A/m^2 , I4- j_0= 1.3*10^{7}A/m^2. b) response for a leakage current density (j_0 =1.3*10^{3}A/m^2) at four different temperatures and η - values : (T=10K , η=15), (T=100K , η=2.5), (T=200K , η=1.75) and (T=300K , η=1.5).

One can see (Fig.2a) that for higher leakage currents, a well-defined maximum near zero swing voltage (i.e. the gate voltage close to the threshold voltage) can be observed. With a decreasing leakage current, the maximum broadens and shifts toward negative swing voltages. A plateau (step-like behavior) is expected for low values of the gate current.

Fig 2b shows the calculated temperature dependence of the photoresponse. One can see that the calculated photoresponse increases with lowering temperature and at lowest temperatures the well defined maximum can be seen. The position of maximum shifts closer to the zero swing voltage (i.e. to the gate voltage close to the threshold).

The temperature dependence of the photoresponse shown in Fig.2b represents a typical device behavior. One can see that the temperature evolution of the width and the amplitude of the photoresponse curves shown in Fig.2 b qualitatively agree with the measured curves shown in Fig.1. (The photoresponse results in Fig.1 are shown as a function of the gate voltage U_g). At low temperatures a well defined maximum is observed and at high temperatures a broad maximum, or rather a step-like behavior near the device threshold voltage is observed.

In summary, the shape of the photoresponse curve defined by Eq.22 and 23 is a function of two main parameters: $\eta k_B T$ that governs the carrier density in the subthreshold region (see Eq.1) and κ, which is a dimensionless parameter related to the leakage current.
The maximum value of photoresponse depends on $\eta k_B T$ only. The width and the position of the maximum depend both on $\eta k_B T$ and κ. For small κ, the photoresponse has a plateau (or step like) behavior near the threshold. For higher values of κ, the photoresponse has a well defined maximum. These rules, although approximate, allow us to understand the photoresponse in most experimental situations described in this work.

We should notice that our model becomes invalid at gate voltages well below threshold when the total number of electrons in the channel becomes small. At such voltages, noise is expected to become very important, leading to an unstable response. The increase of noise at the gate voltages well below threshold was indeed observed experimentally – see Fig.1. Estimates using Eq.1 show that this "small density range" is reached when $(U_g - U_t) << -\alpha \eta k_B T$, where α is of the order 5 to 10. A further decrease of the gate voltage corresponds to the total depletion of the channel and disappearance of the FET response.

Experiment

The devices used in our experiments were typical GaAs/AlGaAs and GaN/AlGaN heterostructure field effect transistors (FETs) with micron and submicron size gates. They were mounted on quartz substrates and wired to variable temperature cryostat sample holders.

GaAs devices were commercially available Fujitsu devices (FHR20X) with the gate width of 50μm and gate length of 0.15μm. The sheet carrier density and electron mobility in the transistor channel were ~10^{12}cm^{-2} and ~2000cm^2/Vs (at 300K), respectively.

The GaN/AlGaN HEMT structures were grown on p-type 6H-SiC substrates. The gate width was 50μm and the gate length was 5μm. The sheet carrier density and electron mobility in the channel of the transistor were ~10^{13}cm^{-2} and ~1500 cm^2/Vs (at 300K), respectively.

The theoretical description, presented above, shows that the parameters necessary to describe the THz photoresponse are: i) carrier mobility (or scattering time) ii) the threshold voltage U_{th}, and iii) the ideality factor η determining the carrier density in the subthreshold region iv) the leakage current. The leakage current was measured simultaneously with the photoresponse. The other parameters were extracted from the current voltage characteristics of the devices following the procedure described in Ref. 1.

The complete set of the current voltage characteristics was measured for each temperature (see Fig.3). The transistor parameters were extracted using the AIM-Spice model. The comparison between the measured data and the FET model is shown in Fig.3. One can see that a good description of the current voltage characteristics was obtained.
Fig.2

Photoresponse of the GaAs/AlGaAs FET at 600GHz - as calculated according Eq.22. a) response at T=300K and for η=1.5, for four different leakage currents. I1 corresponds to the current density j_0=1.3*10A/m^2, I2 - j_0=1.3*10^{3}A/m^2, I3- j_0= 1.3*10^{5}A/m^2 , I4- j_0= 1.3*10^{7}A/m^2. b) response for a leakage current density (j_0 =1.3*10^{3}A/m^2) at four different temperatures and η - values : (T=10K , η=15), (T=100K , η=2.5), (T=200K , η=1.75) and (T=300K , η=1.5).

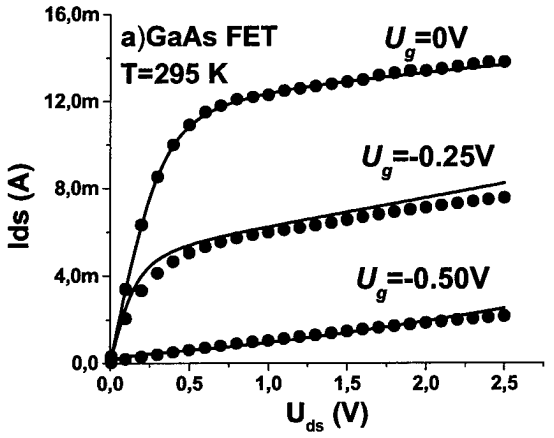

(a)

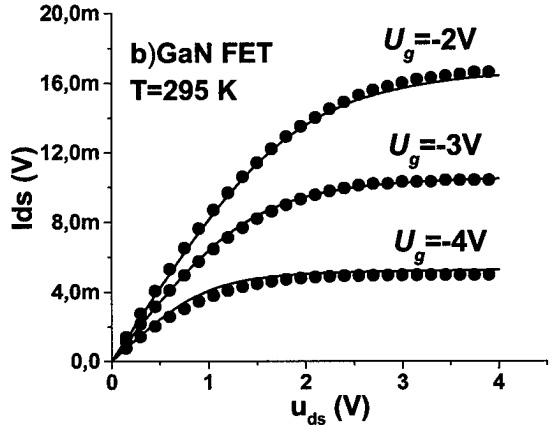

Fig.3. Example of current voltage characteristics of GaAs FETs - a).Gate to source voltages are 0V (the highest curve) – 0.25V (the middle curve) and – 0.50V (the lowest curve). In figure b). Gate voltages are -2V (the highest curve) –3V (the middle one) and –4V (the lowest curve). Points are the experimental results – lines are results of the calculations using AIM-Spice model.

A special care was taken when determining the scattering time (mobility), which is the basic parameter of the theory. Usually in order to determine the mobility, one can use a Hall bar test structure placed somewhere on the wafer along with the devices. However, for micron-size and submicron devices, it is important to determine all the parameters by measurements performed directly on the devices in-situ (not on separate test structures). This is because of the nonuniformity of the wafers leading to a possible spread of the device parameters and (more importantly) because the carriers in submicron devices can undergo some additional scattering related to a small channel size [11].

The electron mobility in the channel was determined from the current voltage characteristics measurements as:

$$\mu_n = \frac{L}{enWR_{Ch}} \qquad (27)$$

where W is the width of the gate, L is the gate length, $R_{Ch} = R_{ds} - R_s$ is the channel resistance, R_{ds} is the measured drain-source resistance at low drain bias, $R_s = R_c + R_{sgd}$ is the channel series resistance, R_c is the contact resistance and R_{sgd} is the resistance of the source-gate, gate-drain regions. At small values of gate voltage, U_g, the concentration n and channel resistance R_{ds} depend on the gate voltage as

$$n = \frac{C(U_g - U_{th})}{e} \quad \text{and} \quad R_{ds} = \frac{L}{en\mu W} + R_s \qquad (28)$$

Therefore the intersection of the dependence of R_{ds} on $(U_g-U_{th})^{-1}$ with the resistance axis yields the resistance R_s. The mobility versus temperature dependences for GaAs and GaN devices, calculated using Eq.27 , are shown in Fig.4a. In both cases, the mobility increases by a factor of 3 to 4 with lowering temperature. The ideality factor η determined from fitting of the $I(V)$ curves is shown in Fig.4b.

The photoresponse measurements were performed using two different experimental setups. The first system used a 100GHz Gunn diode as a radiation source. The maximum output power was 30mW. It was coupled through a ~1.5 m long light pipe system to the sample, which was placed in the exchange gas chamber of the continuous flow cryostat allowing for temperature control and stabilization between 10 and 300K.

The second system used a radiation setup based on a 100 GHz Gunn diode with a frequency doubler ("200 GHz") and tripler ("600 GHz"). The maximum output power was about 3mW (for "200 GHz") and 0.3mW (for "600GHz"). The radiation was optically coupled through the mirror system to the sample placed on the cold finger of the closed cycle cryostat providing sample temperatures in the range 8K-300K.

In all our experiments, the radiation intensity was modulated with a mechanical chopper (30Hz –300Hz range), and the open-circuit source drain voltage was measured by a voltage preamplifier followed by a lock-in. In both systems, the radiation beam was focused to a spot of about 1 mm (which was much bigger than the device dimension). Attenuators were used in order to limit the power in the focused spot to about 0.1 mW in order to avoid heating effects. No special coupling antennas were used, and the radiation was coupled to the devices via the device electrodes metallization pads.

The estimates using the extracted scattering time ($\tau=m\mu/e$) show that for the frequencies f=100 GHz and 200 GHz the basic parameter of the theory $\omega\tau=2\pi f\tau$ was always smaller than unity. For f=600GHz and for the lowest temperatures (T below 30K), $\omega\tau\sim1$ and the resonant feature (marked by an arrow in Fig.1) was observed as a weak maximum superimposed on the nonresonant background [9]. For higher temperatures, only broadband nonresonant detection was observed, see Fig. 1.

The temperature behavior of this non-resonant detection is in agreement with results of calculations shown in Fig. 2. The values of the ideality coefficient η for these calculations were chosen to be close to the experimental ones. One can see that in experiment (Fig.1) and the theory (Fig.2) with lowering the temperature the amplitude of the signal increases and a well defined maximum close to the threshold voltage can be observed. The experimental results are intentionally presented as function of the gate voltage U_g (and not the swing voltage U_0) in order to illustrate the change of the maximum position with the change of the threshold voltage [12] . In

the typical GaAs/AlGaAs devices, the threshold voltage decreased by about 30% -40% with the temperature changing from 300K to 8K.

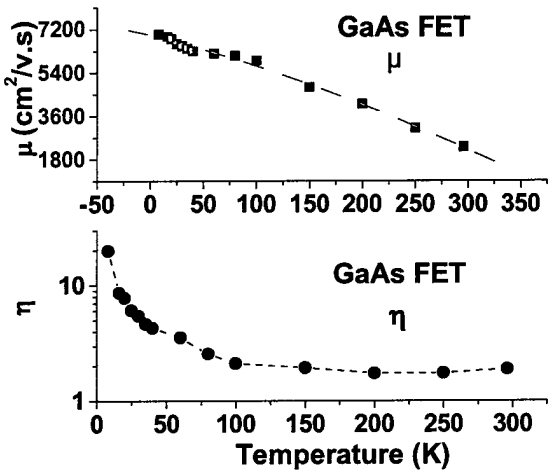

Fig.4 Mobility and ideality factor η versus temperature for 0.15μm gate GaAs/AlGaAs and 5μm gate GaN/AlGaN field effect transistors. Points are experimental results; dotted lines are guides to the eye.

(a)

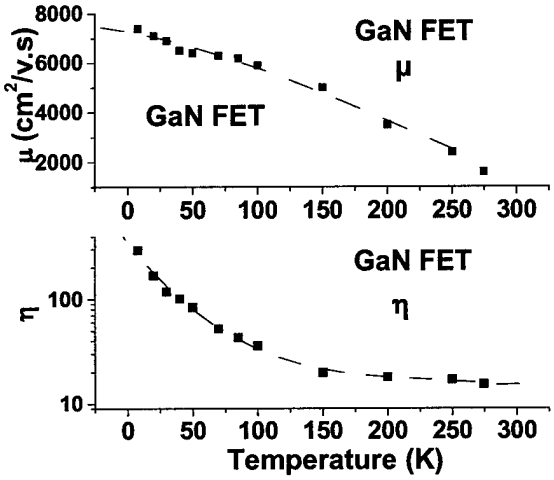

The experimental amplitude of the photoresponse changed with the temperature ~4 times – in approximate agreement with the change of the value of the $\eta k_B T$ parameter (see Fig.4). One can observe however that the calculated curves are always symmetric whereas the measured photoresponse for 8K and 80K has a clearly asymmetric shape. This discrepancy is most probably due to the fact that the theory assumes constant leakage current, while in the experiment the leakage current depends on the gate voltage.

A few examples of direct comparison of the experimental results with the calculations are shown in Fig. 5. The GaAs/AlGaAs FETs photo-response signal registered between the drain and source is presented together with the transfer characteristics. The curves marked as T1 correspond to the transistor with the threshold voltage U_{th}=~0.55V measured at 300K for the frequency 200GHz. The curves marked as T2 and T3 were measured using the 100GHz source . With the exception of the resonance detection at 600GHz , only a very weak dependence of the photoresponse on the radiation frequency was observed. The curve marked as T2 corresponds to

the transistor with U_{th} =-0.42V at 300K. The curves marked as T3 correspond to the same device but measured at a temperature of 10 K, for which the threshold voltage decreased to U_{th} =-0.22V.

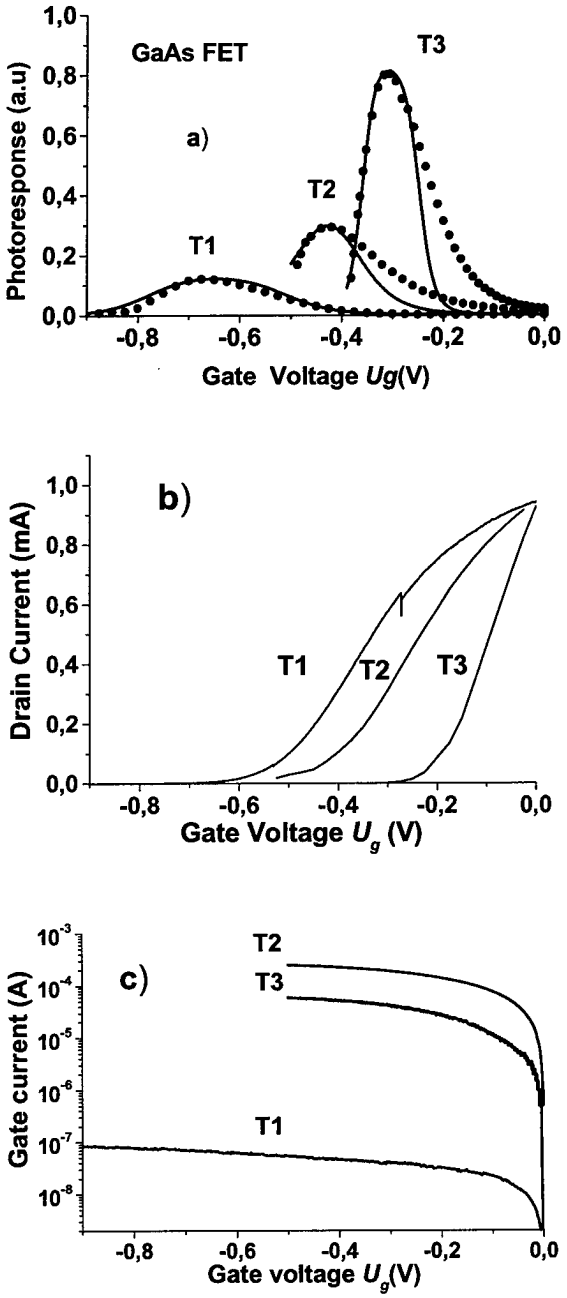

Fig.5Experimental Photo-response a); drain current versus gate voltage U_g b); leakage currents c) measured in three experiments T1, T2, T3 .
Curves marked T1 correspond to the transistor with the threshold voltage U_{th}=~0.55V measured at 300K. Curves marked T2 correspond to the transistor with U_{th} =-0.42V. Curves marked T3 correspond to the same device but measured at a temperature of 10 K, for which the threshold voltage was lower (U_{th} =-0.22V).
In Fig. a) the results of calculations according to Eq.22 are also shown as dotted lines.

One can see that the position of the maximum observed in the nonresonant detection is correlated with the threshold voltage of the device. It is important to note that FET photoresponse extends to the voltages much lower than the transistor threshold. In Fig. 5c, the leakage current versus the gate voltage is shown. In all measurements the leakage current was measured simultaneously with the photoresponse. One can see in Fig.5 that the leakage current

changed monotonously near the threshold voltage. The model presented earlier assumes the constant leakage current. Therefore, in the photoresponse calculations according to Eq.22, we took the value of the leakage current at the transistor threshold voltage U_{th}. Typically for GaAs FETs, the leakage current decreased almost by an order of magnitude when the temperature was lowered from 300K to 10 K.

The curves calculated using Eq. (22) are superimposed on the experimental results. One can see that the overall behavior is correctly described. However, similarly to the case of results for 600GHz (from Fig.1), the calculated curves are always symmetric whereas the experimental photoresponse have a clearly asymmetric shape. These discrepancies are probably due to the fact that the theory assumes the constant gate leakage current, whereas in the actual experimental situations the leakage current increased with increasing gate voltage.

The characteristic plasma wave frequency of the transistor increases with increasing the carrier density in the channel. Therefore, a high electron sheet concentration (up to a few times $10^{13}/cm^2$) in GaN/AlGaN HEMTs makes these devices very promising candidates for applications in plasma wave electronics detectors.

The photo-response of a 5μm gate length GaN/AlGaN FET transistor to 200 GHz radiation was investigated in the temperature range from 8K to 300K. The results for several temperatures are shown in Fig. 6. For each temperature, we also measured the complete set of I-V and transfer characteristics- Fig.3. They allowed us to determine the basic device parameters as described above. The results for the mobility and for the ideality factor are shown in Fig.4. Using these parameters, we calculated the photoresponse according to Eq.23. For comparison, the experiment and the calculation results were both normalized to their maximum values. The change of the photoresponse shape similar to that observed for GaAs FETs can be seen - with increasing temperature the well defined maximum is replaced by a "step-like" curve. One can see that the overall temperature behavior is very well reproduced, confirming the applicability of our model.

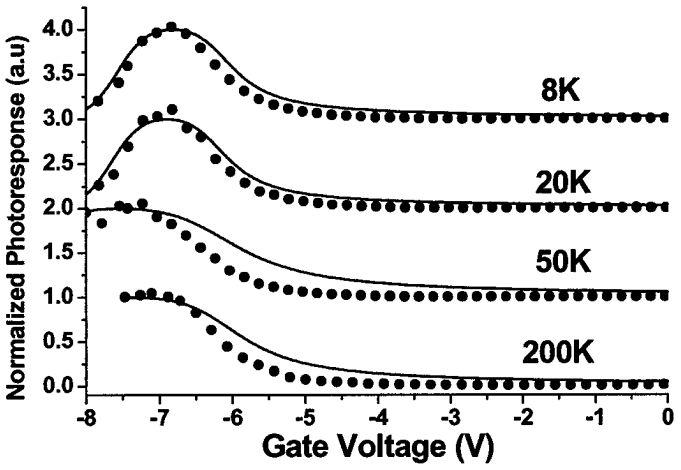

Fig.6 Experimental (points) and calculated (lines) photoresponse of GaN/AlGaN FET for temperatures 8K,20K,50K,200K. The radiation frequency was 200GHz. Results are normalized to their maximum value. For clarity, results for different temperatures were shifted along the Y axis by adding a constant value (1 for 50K, 2 for 20K and 3 for 8K results, respectively).

In conclusion, an experimental and theoretical study of nonresonant subterahertz detection by AlGaAs/GaAs and AlGaN/GaN HFETs in a wide range of temperatures (8-300K) and for frequencies ranging from 100GHz to 600GHz was presented. The new theoretical model, which describes the photo-response below and above the transistor threshold, was developed. It has shown that the gate leakage current suppresses the detector response in the sub-threshold

region leading to a nonresonant maximum in the photoresponse versus gate voltage dependence. Experimental and theoretical results presented in this work allow us to establish the basic physical mechanism of nonresonant THz detection in the subthreshold region.

REFERENCES

1 T. Fjeldly, T. Ytterdal, and M. S. Shur, Introduction to Device and Circuit Modeling for VLSI, John Wiley and Sons, New York, ISBN 0-471-15778-3 (1998)
and M. S. Shur, Introduction to Electronic Devices, Wiley, New York (1996)

2 . M. Dyakonov and M. S. Shur, Shallow Water Analogy for a Ballistic Field Effect Transistor. New Mechanism of Plasma Wave Generation by DC Current, Phys. Rev. Lett. Vol. 71, No. 15, pp. 2465-2468, Oct. 11 (1993)

3 S. J. Allen, Jr., D. C. Tsui, and R. A. Logan, Phys. Rev. Lett., 38, 980 (1977)

4 D. C. Tsui, E. Gornik, and R. A. Logan, Solid State Comm., 35, 875 (1980)

5 P.J.Burke et al Appl. Phys. Lett. vol. 76, 745 (2000)

6 M. Dyakonov and M. S. Shur, Ballistic FET as Tunable Terahertz Oscillator, in Proceedings of 2d International Semiconductor Device Research Symposium, Charlottesville, VA, December, pp. 741-744 (1993)

7 Dyakonov M. I. and Shur M. S., IEEE Transaction on Electron Devices. Vol. 43, No. 10, 1996

8 M. Dyakonov and M. S. Shur, Detection and Mixing of Terahertz Radiation by Two Dimensional Electronic Fluid, in the Proceedings of 22d International Symposium on GaAs and Related Compounds, Cheju, Korea, Aug. 28- Sep. 1, 1995, Institute Conference Series No 145, Chapter 5, pp. 785-790 (1996)

9 W. Knap, Y. Deng, S. Rumyantsev, J.-Q. Lü, M.S. Shur, C.A. Saylor, and L. C. Brunel, Resonant detection of sub-Terahertz radiation by plasma waves in the submicron field effect transistor, submitted to Appl. Phys. Lett.

10 Here we exclude the region of positive gate biases when the gate barrier is collapsed by the forward bias, and the gate leakage becomes dominant.